Computers and Concrete, Vol. 5, No. 2 (2008) 101-116
DOI: http://dx.doi.org/10.12989/cac.2008.5.2.101

Strategies for finding the adequate air void threshold value in computer assisted determination of air void characteristics in hardened concrete

David Duh, Roko Žarnić and Violeta Bokan-Bosiljkov*

University of Ljubljana, Faculty of Civil and Geodetic Engineering, Jamova 2, 1000 Ljubljana, Slovenia

(Received August 14, 2007, Accepted March 2, 2008)

Abstract. The microscopic determination of air void characteristics in hardened concrete, defined in EN 480-11 as the linear-traverse method, is an extremely time-consuming and tedious task. Over past decades, several researchers have proposed relatively expensive mechanical automated systems which could replace the human operator in this procedure. Recently, the appearance of new high-resolution flatbed scanners has made it possible for the procedure to be automated in a fully-computerized and thus cost-effective way. The results of our work indicate the high sensitivity of such image analysis automated systems firstly to the quality of sample surface preparation, secondly to the selection of the air void threshold value, and finally to the selection of the probe system. However, it can be concluded that in case of careful validation and the use of the approach which is proposed in the paper, such automated systems can give very good estimate of the air void system parameters, defined in EN 480-11. The amount of time saved by using such a procedure is immense, and there is also the possibility of using alternative stereological methods to assess other, perhaps also important, characteristics of air void system in hardened concrete.

Keywords: concrete; air void system; linear-traverse method; image analysis; high-resolution flatbed scanner; air void threshold value.

1. Introduction

It is often of great importance to have a microscopic insight into a material, in order to better understand the chemical and physical processes during its exposure to various stress states and/or chemical attack. One such aggressive influence on concrete in cold climates is exposure to freezing and thawing in the presence of moisture and de-icing salts. Both salt crystallization and the freezing of water in the capillary cavities of the concrete produce disruptive pressures in the concrete (Mehta and Monteiro 2006). One of the possibilities of reducing the risk of such damage is air entrainment. The use of an air-entraining agent causes the formation of entrained air bubbles in the cement paste, which, after hardening of the concrete, serve as "escape boundaries" whereto frozen water can expand (Powers 1958). According to such an explanation, an efficient air void system should consist of numerous entrained air voids, located as close as possible to each other. The lower the distance that unstable water must travel to reach the escape boundary, the lower the disruptive pressure generated by such forced flow (Powers 1958). Such an air void system can be obtained

* Corresponding Author, E-mail: vbokan@fgg.uni-lj.si

only by the correct use of a suitable air-entraining agent (Hewlett, *et al.* 2004). Direct verification of adequacy of a formed air void system in hardened concrete can be carried out by using the linear-traverse method (LTM), defined in EN 480-11 (EN 2005). LTM is a quantitative stereological method, traditionally carried out manually on hardened concrete samples observed under the microscope. Because of its direct nature, LTM is one of the most precise methods, and given appropriate samples arguably provide the most useful information about the air void system in hardened concrete (St John, *et al.* 1998). However, the LTM procedure is extremely time-consuming and tedious, and the quality of the results obtained depends on the skill and experience of the operator. For this reason the idea of replacing the human operator in the LTM procedure by some kind of automated system has been popular for many years.

Early microscopical studies of concrete date back to the first half of the 20th century. They proved to be very difficult (St John, *et al.* 1998). Early workers (Parker and Hurst 1935, Brown and Carlson 1936) could hardly examine thin-sections of hydrated cements. The problem was that thin-sectioning the fabric of a concrete was not very practicable until epoxy resins became commercially available in 1946 (St John, *et al.* 1998). Epoxy resin is necessary to bond together the heterogeneous components of concrete so that it can be thin-sectioned. Today, many modern methods are available for the preparation of thin-sections and/or polished sections. Nevertheless, great effort and precision is still needed to achieve sufficient quality. Otherwise, information is lost during the preparation. This is also true for LTM, especially if automatic procedures are to be used. In this case, the specimen surface must be treated in such a way that a better contrast is produced between the air voids and the cement paste. Over the past decades, several researchers (Chatterji and Gudmundsson 1977, Elsen 2001, Pleau, *et al.* 2001, Dequiedt, *et al.* 2001, RDT 2003, Zhang, *et al.* 2005, Jakobsen, *et al.* 2006) have proposed more or less successful automated systems using precise motorization and image analysis to replace the human operator in the procedure of LTM. Although such mechanical automation is quite expensive, the idea of automated systems has remained alive due to the potentially immense reduction in measurement time. Finally, the recent appearance of high-resolution flatbed scanners has made it possible for the procedure to be automated in a fully-computerized and thus cost-effective way. All the mechanical equipment required for automation, coupled with microscope, can now be replaced by a single click of a high-resolution flatbed scanner (Peterson, *et al.* 2001, Peterson, *et al.* 2002, Zalocha 2002, Zalocha and Kasperkiewicz 2005, Carlson, *et al.* 2006). Furthermore, new solutions to some LTM problems are now possible.

2. Automation of LTM

2.1. Identification of the LTM automation problem

In order to automate any quantitative method, unequivocal identification of the investigated phase of the material must be achieved. In case of LTM, the investigated phase consists of the air voids in the matrix of hardened concrete. For such purposes EN 480-11 recommends that the specimen surface is treated in such a way that a better contrast between the air voids and the cement paste is produced. This can be done by first applying ink to the surface of the specimen, and then covering the surface with a contrast material (e.g. zinc paste or barium sulphate), which is pressed into the air voids. Finally, the excess of the contrast material is removed with a scraper. The first problem occurs here - unfortunately the contrast material fills not only the air voids but also any other

surface defects, such as cracks, micro-cracks, voids in the aggregate, etc. Thus, unequivocal identification of the investigated phase is not achieved. The problem can be greatly reduced by increasing the quality of the specimen surface preparation. However, even extremely careful grinding will not solve the problem of possible macro-cracks, poor compactness of the cement paste, or voids in the aggregate. If this is the case, such surface defects should not be neglected.

The second problem occurs when a human operator must, whether directly or indirectly, choose a threshold value for identification of the air voids. This is because, however good the contrast enhancement, the specimen surface will never appear ideally black and white. It will consist of dark areas, which indicate the aggregate and cement paste, and brighter areas, which mostly indicate air voids, as shown in Fig. 1. If the threshold value is chosen too conservatively, the automated system will not stop at air voids which are not perfectly bright white, and/or will not capture the whole air voids. The result would be an underestimation of the actual form of the air void system. In the opposite case, the automated system would overestimate the actual state by identifying every brighter area as an air void. This problem can be reduced by increasing the quality of contrast enhancement of the specimen surface, as shown in Fig. 1, but the results of automated systems still greatly rely on the experience of the human operator. Some researchers (Jakobsen, *et al.* 2006), however, have stated that the measurements are not very sensitive to some variations in the threshold setting. Such statements can be strongly misleading, since there is no definition of the magnitude of these variations nor any image capturing brightness and contrast settings given. The automated procedure of the LTM is highly sensitive, firstly, to the quality of the sample surface preparation, secondly, to the selection of probe system, and lastly to the experience of the human operator, when choosing the proper threshold value for the identification of air voids. In the following chapters two ideas are proposed about how to eliminate the human operator also in this last phase of LTM automation – the selection of the adequate air void threshold value.

2.2. Ideas about how to overcome the LTM automation threshold problem

The first idea is based upon the rules of planar stereology. Since it is connected directly to the image histogram of the captured specimen surface, we named it HST method. The second idea is

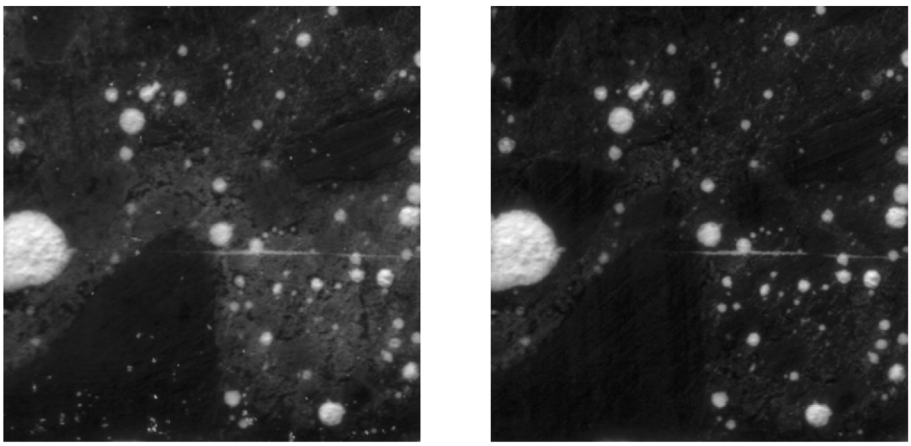

Fig. 1 The effect of higher quality of contrast enhancement (on the right) of the specimen surface

connected to the linear stereological method used in EN 480-11. As this idea is in fact parametrization of LTM results, where the parameter is image threshold value, we named it THR method.

2.2.1. LTM principal parameters

Firstly, let us introduce the LTM principal parameters, defined in EN 480-11. These are: total air content A, micro air content A_{300}, specific surface of air void system α and spacing factor $\overline{L}$. All the parameters are calculated from the following data obtained during the test procedure: total length of traverse across solid phases T_s, total length of traverse across air voids T_a, total number of chords across air voids N and cement paste content by volume P calculated from the mix proportions. The total air content is defined as proportion of the total volume of the concrete that is air voids and is calculated from the following expression:

$$A = \frac{T_a \cdot 100}{T_{tot}} \tag{1}$$

where $T_{tot} = T_s + T_a$. The micro air content is attributed to air voids of 300 μm in diameter or less and is obtained from the estimated air void distribution. The specific surface of air void system is representing the total surface area of the air voids divided by their volume and is calculated from the following stereological expression valid for any system of spherical voids:

$$\alpha = \frac{4}{\overline{l_c}} = \frac{4 \cdot N}{T_a} \tag{2}$$

where $\overline{l_c}$ represents the average chord length. Finally, the spacing factor is related to the maximum distance of any point in the cement paste from the periphery of an air void, measured through the cement paste, and is calculated from the following relationships:

$$\overline{L} = \frac{3[1.4(1 + P\,A)^{1/3} - 1]}{\alpha}, \text{ when } P/A > 4.342 \tag{3}$$

$$\overline{L} = \frac{P \cdot T_{tot}}{400 \cdot N}, \text{ when } P/A \leq 4.342 \tag{4}$$

2.2.3. HST method

The most fundamental rule in stereology is that the volume fraction V_V of a certain phase within the structure can be measured by the area fraction S_S of that phase on a random section through the structure (Russ and Dehoff 2000). This relationship is known to be proposed by Delesse in 1848 (St John, *et al.* 1998) and can be expressed mathematically as:

$$V_V = S_S \tag{5}$$

If the contrast-enhanced surface of a specimen cut from a hardened concrete sample is captured with a flatbed scanner, a histogram of the specimen surface can be obtained. This histogram consists of three base histograms, if the RGB technique is used. Since the chosen contrast enhancement of the specimen surface is colourless, the grayscale technique should be sufficient. In this case the histogram presents the frequency distribution of 256 grey values x in the captured specimen surface image, from white (x = 255) to pitch black (x = 0), as shown in Fig. 2 (upper-left corner). The unit of the captured grayscale image is 1 pixel. In case of a high-resolution 2400 dpi flatbed scanner, 1

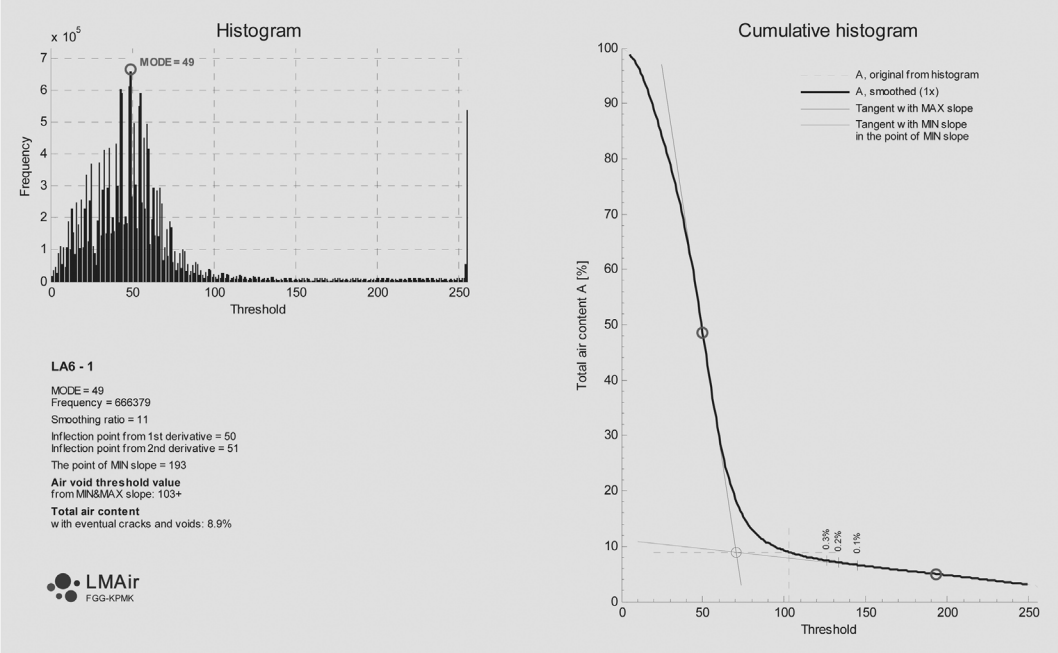

Fig. 2 Screenshot from the prototype application LMAir – the proposed HST method

pixel represents approximately 10 μm, which should be enough for the purposes of the LTM. This is because the voids below 10 μm already represent capillary pores (St John, Poole and Sims 1998), and could therefore be easily misidentified as entrained air voids if higher resolutions are used.

After the grayscale histogram is obtained, the idea of the proposed HST method is firstly to convert the histogram to a cumulative form in the direction of darker grey values, as shown in the following algorithm, where *ThrFrq* represents the vector of the histogram frequencies and *ThrCum* the vector of cumulative histogram values:

```
ThrCum(256) = ThrFrq(256)
for x=1:255
    ThrCum(256-x) = ThrCum(256-x+1) + ThrFrq(256-x)
end
```

The obtained cumulative curve *ThrCum*(x), shown in Fig. 2 (right diagram), represents the area fraction of all pixels from the grayscale interval [x, 255] in the captured image of the contrast-enhanced specimen surface. According to Delesse's relationship, Eq. (5), every value *ThrCum*(x_i) should therefore provide a good estimate of the volume fraction of the phase represented by this grayscale interval [x_i, 255]. Therefore, if we choose the correct threshold value x_a, such that represents the air voids in the captured image, the value *ThrCum*(x_a) will represent the estimated total air content A:

$$ThrCum(x) = S_S(x) = V_V(x) \rightarrow V_V(x = x_a) = ThrCum(x_a) = A \tag{6}$$

In order to eliminate the need for a human operator in this phase, too, of the automatic procedure, the proposed HST method is able to choose this threshold value x_a automatically. The obtained

cumulative curve, shown in Fig. 2 (right diagram), has an approximate linear slope in the area of higher threshold values, which is due to the contrast enhancement, which cannot produce an ideally black and white surface. The cumulative percentage of brighter pixels in the captured grayscale image will therefore increase slowly as the threshold interval [x, 255] is increased. As can be seen in Fig. 2 (right diagram), the linear slope of the cumulative curve will end at a certain point, and a non-linear ascent will follow. At this point, the pixels with the corresponding threshold value will start to represent the non-contrasted areas, which are cement paste and aggregate. Also, the cumulative curve will always end at 100%, as this is the area percentage of all possible pixels in the captured image. The results of our research showed that the end point of the discussed linear slope on the right-hand side of the cumulative curve is more obvious when the specimen surface preparation has been carried out with higher quality. Furthermore, in this case the end point can provide a good estimate of the air voids identification threshold value x_a.

In the prototype MATLAB application, named LMAir by the authors, the proposed HST method firstly reads the grayscale histogram of the captured contrast-enhanced specimen surface. It then obtains the cumulative curve of the histogram and determines the end point of the linear slope on its right-hand side. This is done by analyzing the curve derivatives, where sufficient smoothing of the curve and curve derivatives has to be done in order to reduce the noise. After the minimum slope of the cumulative curve has been obtained, the end point of the discussed linear area is estimated by observing the deviation of the curve $ThrCum(x)$ from the minimum slope line $y_{MIN}(x)$, as shown in the following algorithm, where tolerance *tol* is a small number to be defined by careful validation, as presented in the following chapters:

```
x = 1
while (ThrCum(x)-yMIN(x)) > tol
    x = x + 1
end
xa = x
```

Finally, the end point of the discussed linear area is saved as the air void threshold value x_a for the final evaluation phase. In this phase the maximum expected value of the total air content A is also obtained.

2.2.3. THR method

Taking into account the nature of the already discussed cumulative curve related to the total air content A, similar inflection points and linearity areas could also be expected for the two other LTM parameters $\overline{L}$ and α. That is, of course, if $\overline{L}$ and α curves are obtained as functions of the threshold value x, or rather, as functions of the threshold interval [x, 255]. For such a task mechanical automated systems would probably require even more time than the whole of the traditional manual procedure. However, the above-discussed computer-automated system with a flatbed scanner requires only 5-10 minutes to complete this task. This is due to the fact that, when capturing the specimen surface with a flatbed scanner, this has to be done only once. The captured specimen surface is therefore ready to be analyzed by means of image analysis software as many times as is necessary. For this purpose it is necessary to construct a script for an image analysis program, such as ImageJ (NIH 2004), which will analyze the captured image and calculate all of the LTM parameters, as defined in EN 480-11, for each selected threshold interval [x, 255]. The results should then be presented in diagram form, as shown in Fig. 3.

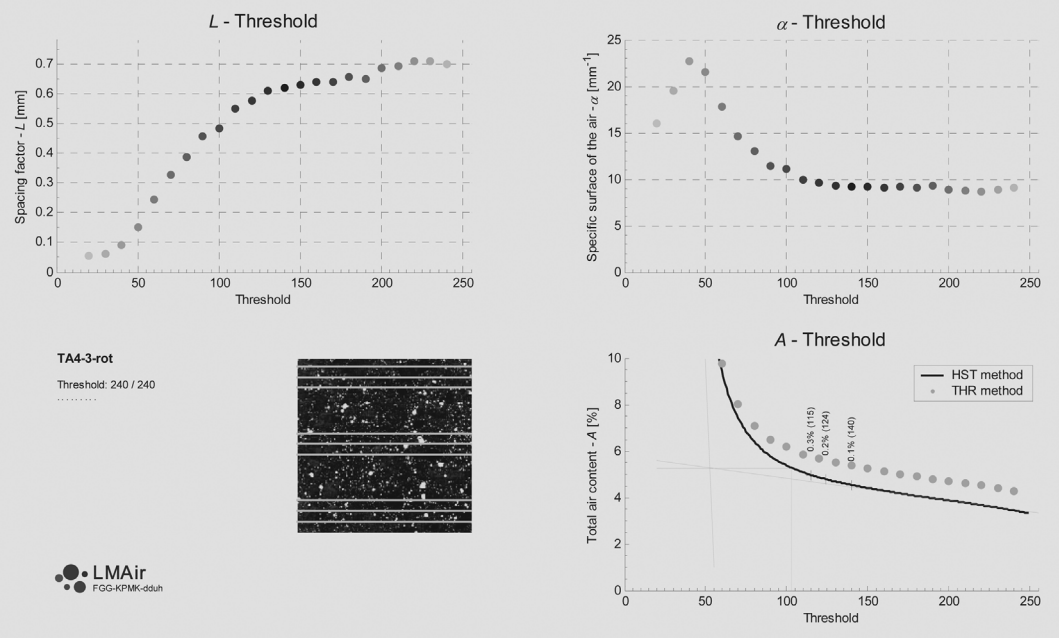

Fig. 3 Screenshot from the prototype application LMAir – the proposed THR method

To explain the idea of the proposed THR method, let us first analyze the α-Threshold curve (Fig. 3, upper-right diagram). The approximate linearity in the right-hand area can usually be identified. As already explained, this is the area of brighter grey pixels in the captured image of the contrast-enhanced specimen surface, which mostly indicates contrasted air voids. As the air voids are not of equal size and depth, they have a different glow, and thus different greyness. In principle, the bigger the void, the brighter the glow. But why again the linearity, considering that we are observing parameter α this time? The answer to this question is slightly more complex than the one for parameter A in previous chapter. However, it does also have a physical background. The specific surface of a geometrical body α_i is by definition the ratio between its surface area P_i and its volume V_i. The specific surface of a sphere, which is a good representation of entrained air voids, is therefore:

$$\alpha_o = \frac{P_o}{V_o} = \frac{4\pi r^2}{\frac{4}{3}\pi r^3} = \frac{3}{r} \tag{7}$$

where r is the sphere radius. According to Eq. (7), smaller air voids have larger specific surfaces. Hence, a system of mostly small air voids has a larger specific surface than a system having the same number of larger air voids. Great care should be taken that the number of air voids is never neglected in calculations of the specific surface of an air void system, as defined by Eq. (2). According to Eq. (2), the specific surface of an air void system should rise greatly, if only small air voids are added to the current system. If α is to be kept constant, when new smaller air voids are added to the system, then existing air voids should simultaneously get larger in order to balance the increasing numerator of the α fraction. And this is exactly what happens when the [x, 255] threshold interval is increased. Due to the contrast enhancement, proposed in EN 480-11, and capturing optical effect of a flatbed scanner, contrasted air voids usually appear brighter in the

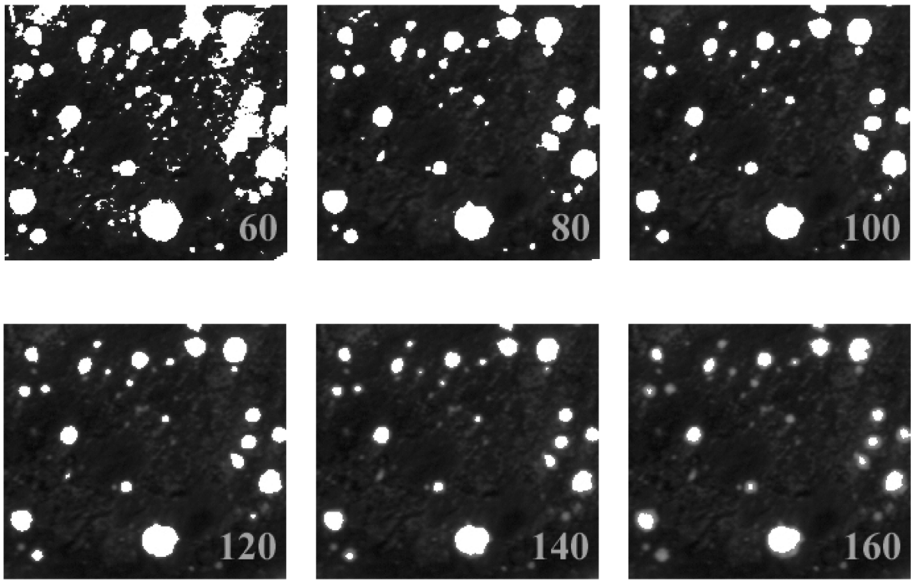

Fig. 4 Identification of the air voids (pure white) in a small section of the contrast-enhanced specimen surface according to the chosen threshold interval [*x*, 255]

centre. For this reason when increasing the [*x*, 255] threshold interval, new smaller air voids with a dimmer glow are constantly added to the system, and the existing air voids in the current system get larger, as be seen in Fig. 4. Thus, the specific surface of the air void system α remains almost constant (it can also show a slight linear slope). Again, this linearity ends at the point where, when increasing the [*x*, 255] threshold interval, the true edges of the air voids are reached. By further lowering of the threshold value *x* only new small areas of darker grey pixels are added to the current system, causing α to increase greatly. However, it does not continue to increase indefinitely, since, as the [*x*, 255] threshold interval is further increased, some bigger identified areas finally start to merge. Consequently, the number of identified areas *N* starts to drop and thus also α. The results of our research have shown that the end point of the discussed linearity of the α-Threshold curve is more obvious when specimen surface preparation has been carried out with higher quality. Furthermore, in this case the end point is also a good estimate of the air voids identification threshold value x_a. It can be calculated by analogue procedure as described in the proposed HST method.

The air voids identification threshold value x_a can usually also be obtained from the $\overline{L}$-Threshold curve (Fig. 3, upper-left diagram) by following the analogue procedure as described above. The reason is that the spacing factor $\overline{L}$ is usually inversely proportional to the specific surface of air α, as can be seen from the relationships in Eqs. (3)-(4).

Following the same procedure as discussed in the proposed HST method, the air voids identification threshold value x_a can also be obtained from the *A*-Threshold curve (Fig. 3, bottom-right diagram). This curve can also serve as the control curve for the HST method, or vice versa. However, there will always be a slight difference between these two curves, as the HST method uses the planar stereological method, where the whole specimen surface is taken into account. On the other hand, the THR method is based on the linear stereological method, where only the air

voids intersected by the selected probe system on the specimen surface are taken into account. In principle, the more extensive the probe system is, the smaller the difference will be between the THR *A*-Threshold curve and the HST *A*-Threshold curve.

The presented diagrams in Fig. 3 also prove the high sensitivity of LTM parameters to the chosen threshold value *x*. It can be seen from the $\overline{L}$-Threshold and the α-Threshold curve that already some small variations in the threshold setting, such as 10 grayscale units, can cause up to 10% difference in the estimation of parameters $\overline{L}$ and α, since the correct air void threshold value x_a lies at the end of the linear areas of the discussed curves. Parameter *A* is approximately half less sensitive to this threshold setting. These estimations of the LTM parameters sensitivity, of course, depend greatly on the capturing brightness and contrast settings. However, the relative sensitivity of the LTM parameters to the threshold settings is always the same. Furthermore, by choosing higher contrast settings for capturing the specimen surface, in order to lower the absolute sensitivity of the LTM parameters to the threshold settings, potentially important data are lost.

Finally, the result of the two proposed methods should be four estimated values for x_a, i.e., one from the HST method and three from the THR method. The mean value $\overline{x_a}$ of all four obtained values should be calculated and taken as the threshold setting for the final evaluation of all LTM parameters.

3. Results of tests performed to validate the proposed ideas

3.1. Materials and equipment

It is generally agreed by researchers working on the development of different LTM automated systems that any kind of LTM automated method has to be fully validated before it can be used as a routine procedure. Such a validation must necessarily include comparisons between the values obtained from image analysis and those obtained from the EN 480-11 visual examination for a large number of concrete mixtures, covering a wide range of mixture compositions and air ratios (Pleau, Pigeon and Laurencot 2001). Therefore, six different concrete mixtures were chosen in order to test the proposed ideas for overcoming the LTM automation problem described in the previous chapters. The chosen concrete mixtures cover the air content interval from 4% to 10% (one of them being a

Table 1 Mixtures proportions (kg/m^3) and the air content of the fresh concrete

Mixtures	LA10	LA6	LA4	TA4	CA4	EFn
Aggregate	1429	1467	1500	1499	1499	1472
Cement	403	413	422	422	422	396
Limestone powder (Type I)	244	250	256	–	–	–
Limestone powder (Type II)	–	–	–	255	–	–
Limestone powder (Type III)	–	–	–	–	255	–
Fly ash	–	–	–	–	–	214
Superplasticizer	4.01	4.11	4.20	5.15	4.40	4.15
Air-entraining agent	0.68	0.65	0.55	0.42	0.97	–
Water	157	161	165	165	165	188
Air content*	9.0%	6.6%	4.5%	4.5%	4.5%	4.5%

*Calculated from the fresh concrete density according to EN 12350-6.

non-aerated concrete mixture), and a range of four different types of mineral additions. The mixtures details are given in Table 1.

For the purposes of LTM three standard cube (100 mm) specimens were cast from each concrete mixture. Preparation of test surfaces was carried out according to EN 480-11. However, the contrast enhancement, as proposed in EN 480-11, was studied in detail during the research. For wet grinding, magnesite abrasives were used. After the fine lapping had been completed, the test surfaces were carefully cleaned in an ultrasonic bath at a frequency of 40 kHz and a HF peak power of 300 W. Manual microscopic examination was then carried out by means of a HIROX KH-3000 optical microscope system, at magnification of 100x. Side lighting was used to obtain better identification of the air voids at shallower depths. The test surfaces were then contrast enhanced with black stamp (water insoluble) ink, zinc paste and gypsum powder, as proposed in EN 480-11. The excess gypsum and zinc paste was removed with a fine razor blade. All the test surfaces were captured with a high-resolution flatbed scanner (2400 × 2400 dpi) immediately after the contrast enhancement had been completed, in order to avoid zinc paste contraction in the air voids. The captured images were saved in TIFF format to avoid any loss of detail due to the possible higher compression of some other image formats. Finally, the captured images were analysed using the prototype MATLAB application LMAir, based on the two proposed ideas, HST and THR. The application uses the open source image analysis software ImageJ (NIH 2004).

3.2. Comparison between the prototype application LMAir and the manual LTM

For the purposes of manual microscopic examination, the lines of the chosen probe system were softly engraved using a sharp razor blade. After the test surface had been contrast enhanced, these finely engraved lines were also partly filled with the contrast material, as it can be seen in Fig. 1.

Table 2 Values of LTM parameters for all test mixtures as obtained from manual microscopic examination and from the prototype application LMAir for different quality of contrast enhancement

	Mixtures	LA10	LA6	LA4	TA4	CA4	EFn
Manual LTM	Total air content A [%]	10.40	7.74	5.38	5.24	4.60	3.66
	Specific surface α [mm^{-1}]	15.15	12.51	11.81	11.05	10.44	14.36
	Spacing factor $\bar{L}$ [mm]	0.258	0.383	0.484	0.524	0.587	0.479
	Micro air content A_{300} [%]	2.33	1.55	0.98	0.59	0.66	0.91
Automated LMAir (low quality of contrast enhancement)	Total air content A [%]	10.23	–	–	–	5.46	3.73
	Specific surface α [mm^{-1}]	16.28	–	–	–	16.11	16.66
	Spacing factor $\bar{L}$ [mm]	0.245	–	–	–	0.352	0.410
	Micro air content A_{300} [%]	2.56	–	–	–	1.38	1.03
Automated LMAir (high quality of contrast enhancement or 1 pix elimination)	Total air content A [%]	10.50	7.77	5.50	5.55	5.05	3.84
	Specific surface α [mm^{-1}]	13.72	12.20	11.56	11.09	13.73	13.99
	Spacing factor $\bar{L}$ [mm]	0.283	0.397	0.493	0.508	0.433	0.482
	Micro air content A_{300} [%]	2.24	1.46	1.09	0.89	1.27	1.03

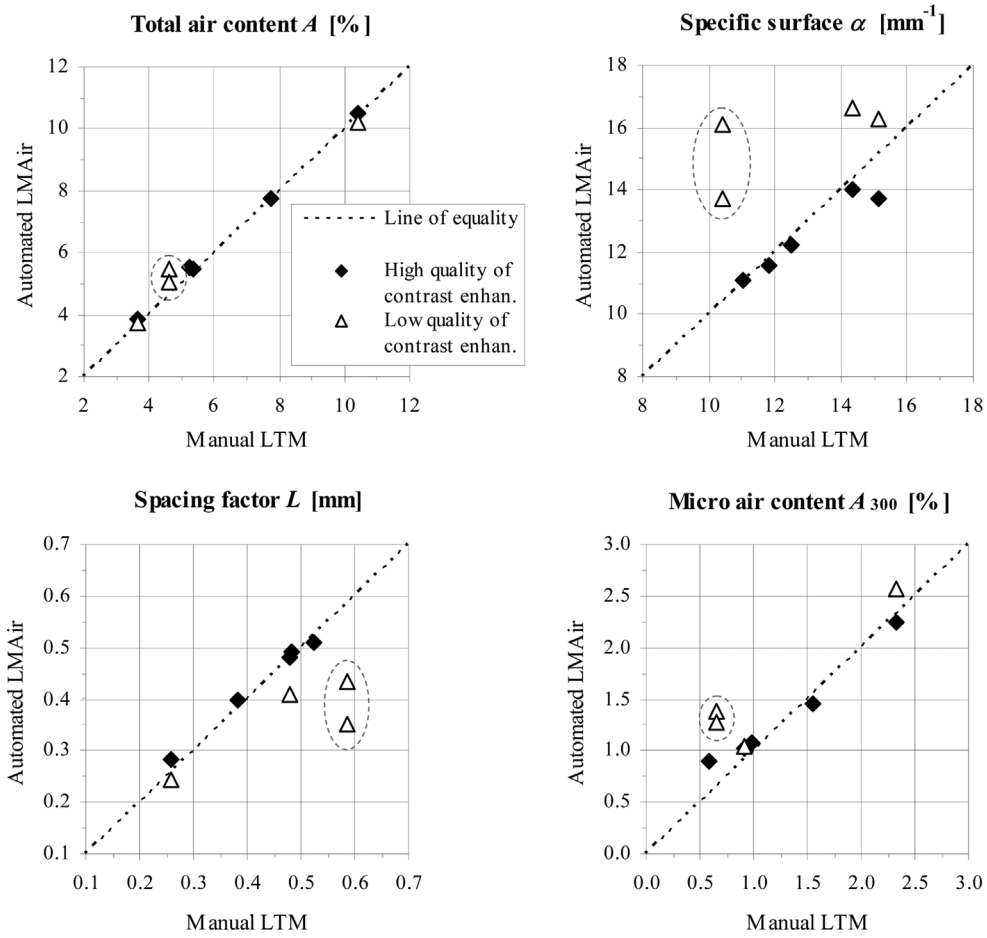

Fig. 5 Relationship between LTM parameters for all test mixtures as obtained from manual microscopic examination and from the prototype application LMAir for different quality of contrast enhancement

This was beneficial for the validation of the proposed linear THR method, since the lines of the probe system could be chosen in almost the same way. However, for the validation of the proposed planar HST method, these partly contrasted lines created an error on the test surface. This error was carefully considered in the HST method as the maximum expected value of the total air content *A*. The results of the comparison between the values obtained by using the prototype application LMAir and those obtained by manual microscopic examination are presented in Table 2 and Fig. 5.

Fig. 5 shows that the prototype application LMAir can provide a very good estimate of all the LTM parameters, though only in the case of high-quality specimen surface preparation. If grinding and contrast enhancement of the test surface are carried out with poor quality, the results obtained by using LMAir are almost useless. Furthermore, great care should be taken, as in such situations the automatically obtained results will always overestimate the actual form of the air void system. This is because poor quality of contrast enhancement means larger amount of small bright artefacts on the test surface, which will be identified by the computer as small air voids. Hence,

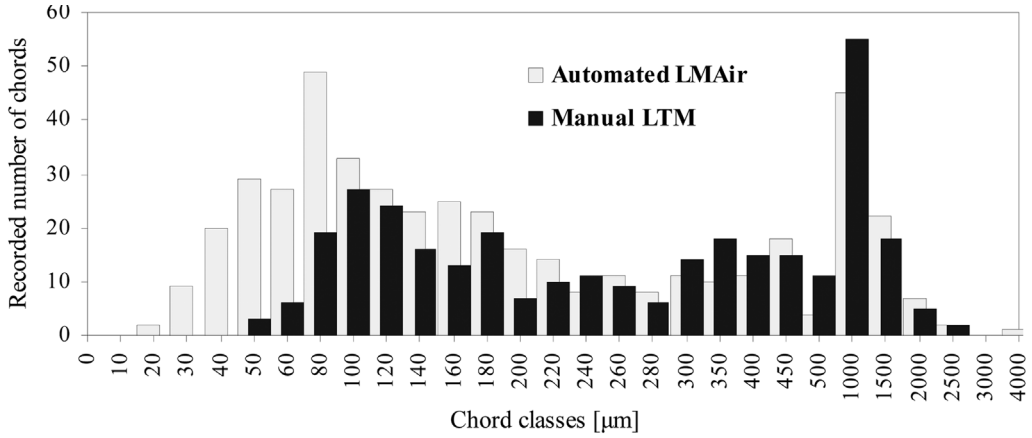

Fig. 6 Comparison between CA4 chord frequencies obtained from manual LTM and automatic LMAir with 1 pixel elimination

the result will show a slightly greater total air content and a much better, i.e. lower, spacing factor. A good example of such a situation is provided by the mixture CA4 (encircled in Fig 5). One of the methods which was used to try to eliminate the small artefacts from the CA4 surface was the elimination of all identified chords of 1 pixel (~10 μm). As seen from Table 2, the results obtained in such a way were much closer to those obtained with manual LTM, but the relative error was still very high, around 25%. Certainly, such a poorly contrast-enhanced test surface also contains numerous artefacts with a size greater than 1 pixel. To verify this, it is best to compare the CA4 chord frequencies obtained from both the manual LTM and the automated LMAir with 1 pixel elimination (Fig. 6). It can be seen from the diagram in Fig. 6 that there are still a large amount of artefacts of sizes 2-8 pixels on the poorly contrast-enhanced CA4 surface. The further elimination of automatically identified chords of size at least 2-6 pixels would therefore solve the problem of potential artefacts for CA4. However, such a solution would cause a large error in all other cases, where smaller air voids are actually present. During our research it soon became clear that the safest, if not the only way to eliminate such artefacts is by improving the quality of the specimen surface preparation. However, this may not always be possible. In case of concretes with a weak cement-paste matrix, sand grains might be plucked from the surface during lapping, which would result in scratching of the surface and undercutting of the paste around the harder aggregate particles. Friable particles of aggregate can also cause difficulties. In such instances the hot waxing procedure proposed in ASTM C 457 (ASTM 1998) might be helpful.

During the validation of LTM automated systems, by comparing the results obtained from image analysis and those obtained by visual examination according to EN 480-11, it is necessary to bear in mind the fact that LTM is very sensitive to the heterogeneity of the material and to the selection of the probe system. EN 480-11 therefore defines a minimum total traverse length of 2400 mm. If a simulation of several LTM is made on the chosen specimen over a total traverse length of 2400 mm, each time with slightly different positions of the chosen traverse lines, the obtained results vary up to ±10% from the average value, as can be seen in Fig. 7. This LTM simulation was carried out for two different mixtures, LA10 and TA4, with the highest and the lowest total air contents,

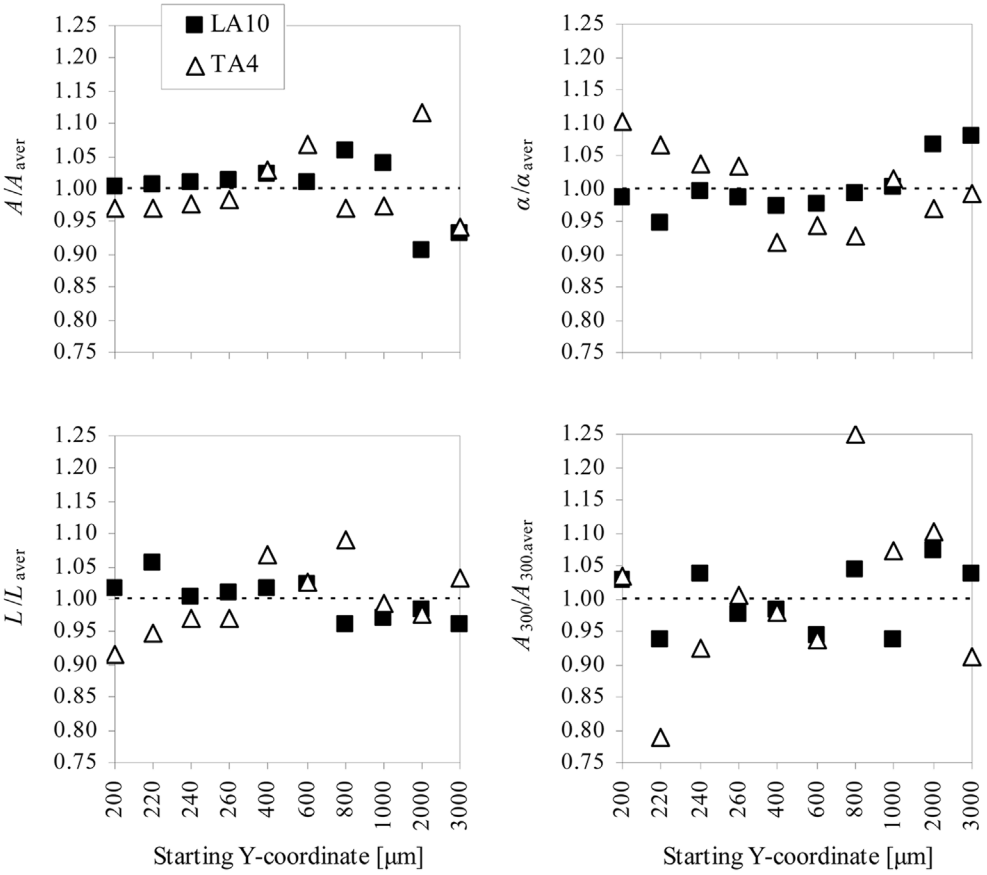

Fig. 7 The sensitivity of LTM to the selection of positions of the traverse lines over a total traverse length of 2400 mm

respectively. The traverse line positions were shifted each time in steps of 20 μm, 200 μm and 1000 μm. The total traverse length was always 2400 mm. From Fig. 7 it can be seen that for the parameter A_{300} a deviation of at least 25% from the average value can be expected, just by selecting the position of the traverse lines slightly differently. However, this is also due to the not very appropriate definition of this parameter in EN 480-11, which has been explained at greater length in (Duh, *et al.* 2006). If more reliable results for LTM parameters are needed, the total traverse length should be increased. In the case of a doubled minimum total traverse length of about 4800 mm, 5% deviation from the average values could be expected for all the LTM parameters, except for A_{300}. Yet this would also double the time needed to carry out the LTM manually. That means an additional 15-20 man-hours of work. However, using a computer-automated system, such as the prototype LMAir, the additional 2400 mm of length of the traverse line could be analysed in just a few minutes.

4. Conclusions and further possibilities

The results of our research have led us to the following conclusions:

- In order to perform LTM manually using a microscope, approximately 15-20 man-hours per test are needed. By increasing the size of the probe system, in order to obtain more reliable results, the working time increases linearly at an approximate rate of 30 minutes per 100 mm of additional length of the traverse line. Using an automated system, consisting of a high-resolution flatbed scanner and image analysis software, LTM can be performed at least 4 times faster, almost regardless of the chosen size or type of probe system.
- LTM parameters obtained from automatic procedures are highly sensitive to the threshold settings for the identification of air voids on the contrast-enhanced specimen surface.
- The proposed ideas to overcome the LTM automation problem by means of choosing the correct air void threshold value proved to be adequate in most cases. They are independent of human effects, and in the case of high-quality test surface preparation they can provide a very good estimate of all the LTM parameters.
- In the validation process of any automated system it should be borne in mind that, with a minimum total traverse length (2400 mm), the LTM, as a linear stereological method, shows approximately 10% deviation from the average values, if only slightly different positions of the traverse lines are chosen.

Furthermore, such a type of automation, where the whole specimen surface is pre-captured at once by a flatbed scanner, also makes it much easier for the planar stereological methods to be used. Planar analysis has many advantages over linear stereological methods in such applications. Firstly, it is easier to estimate the volume fraction of a phase directly from its area fraction rather than indirectly from linear measurements. Secondly, the whole specimen surface can be analyzed in less than a minute, not just the regions along the selected traverse lines. However, difficulties occur if the air void distribution needs to be estimated. This mathematical problem is often regarded as ill-posed.

Finally, when estimating the LTM parameters, it should also be taken into consideration that the discussed Powers spacing factor may, in fact, not be the best representation of the air void system in hardened concrete, nor a parameter upon which the frost-thaw resistance of concrete could be accurately predicted. Nowadays, when planar image analysis can be carried out just as fast as linear analysis, the development of new alternative parameters is possible. The motivation is the even more accurate representation of the actual air void system in hardened concrete. Investigations of the possible stacking of air voids could be interesting, in order to predict the frost-thaw resistance of concrete even more accurately.

Acknowledgements

The paper presents the results of research work which was performed within the framework of a PhD study financed by the Research Agency and the University of Ljubljana, Faculty of Civil and Geodetic Engineering. BION, the institute for Bioelectromagnetics and New Biology provided helpful information regarding image analysis. The support of all these organizations is hereby gratefully acknowledged.

References

ASTM C 457 (1998), "Standard test method for microscopical determination of parameters of the air-void system in hardened concrete", *Annual Book of ASTM Standards*, 240-253.

Brown, L.S. and Carlson, R.W. (1936), "Petrographic studies of hydrated cements", *Proceedings of the American Society of Testing Materials* **36**, Part II, 332-350.

Carlson, J., Sutter, L. L., Van Dam, T. J., and Peterson, K. W. (2006), "Comparison of flatbed scanner and rapidair 457 system for determining air void system parameters of hardened concrete", *J. Transportation Research Board*, TRB, **1979**, 54-59.

Chatterji, S. and Gudmundsson, H. (1977), "Characterization of entrained air void system in concrete by means of an image analysis microscope", *Cement Concrete Res.*, **7**, 423-428.

Dequiedt, A.-S., Coster, M., Chermant, L., and Chermant, J.-L. (2001), "Distances between air-voids in concrete by automatic methods", *Cement Concrete Compo.*, **23**, 247-254.

Duh, D., Leskovar, R. T., Žarnić, R., and Bokan-Bosiljkov, V. (2006), "Validation and automation of linear-traverse method for the estimation of the adequacy of air-void system in hardened concrete", *Proceedings of 28th Congress of Structural Engineers of Slovenia (in Slovenian)*, Bled, Slovenia, October, 197-206.

Elsen, J. (2001), "Automated air void analysis on hardened concrete: Results of a European intercomparison testing program", *Cement Concrete Res.*, **31**, 1027-1031.

EN 12350-7 (2001), "Testing fresh concrete – Part 7: Air content – Pressure methods", *European Standard*, CEN.

EN 480-11 (2005), "Admixtures for concrete, mortar and grout – Test methods – Part 11: Determination of air void characteristics in hardened concrete", *European Standard*, CEN.

Hewlett, P. C. et al. (2004), *Lea's Chemistry of Cement and Concrete*, Fourth Edition, Elsevier.

Jakobsen, U. H., Pade, C., Thaulow, N., Brown, D., Sahu, S., Magnusson, O., De Buck, S. and De Schutter, G. (2006); "Automated air void analysis of hardened concrete – a Round Robin study", *Cement Concrete Res.*, **36**, 1444-1452.

Mehta, P. K. and Monteiro, P. J. M. (2006), *Concrete: Microstructure, Properties and Materials*, Third Edition, McGraw-Hill.

NIH (2004), *ImageJ*, Image Processing and Analysis in Java, US National Institutes of Health. (http://rsb.info.nih.gov/ij/)

Parker, T.W. and Hirst, P. (1935), "Preparation and examination of thin sections of set cement", *Cement and Cement Manufacture*, **8**(10), 235-241.

Peterson, K. W., Swartz, R. A., Sutter, L. L., and Van Dam, T. J. (2001), "Hardened Concrete Air Void Analysis with a Flatbed Scanner" *J. the Transportation Res. Board*, TRB, **1775**, 36-43.

Peterson, K., Sutter, L., and Van Dam, T. (2002), "Air void analysis of hardened concrete with a high-resolution flatbed scanner", *Proceedings of the 24th International Conference on Cement Microscopy*, San Diego, California, 304-316.

Pleau, R., Pigeon, M. and Laurencot, J.-L. (2001), "Some findings on the usefulness of image analysis for determining the characteristics of the air-void system on hardened concrete", *Cement Concrete Compos.*, **23**, 237-246.

Powers, T. C. (1958), "The physical structure and engineering properties of concrete", *Bulletin 90*, Portland Cement Association, Skokie, IL.

RDT (2003), *Advanced Research of an Image Analysis System for Hardened Concrete*, Research Investigation 98-006, Missouri Department of Transportation.

Russ, J. C. and Dehoff, R. T. (2000), *Practical Stereology*, Second Edition, Kluwer Academic, Plenum Publishers, NY.

St John, D. A., Poole, A. W., and Sims, I. (1998), *Concrete Petrography: A handbook of investigative techniques*, Arnold, London.

Zalocha, D. (2002), "Image analysis as a tool for estimation of air-void characteristics in hardened concrete: example of application and accuracy studies", *Workshop on Structural Image Analysis in Investigation of Concrete*, Warsaw, Poland, October.

Zalocha, D. and Kasperkiewicz, J. (2005), "Estimation of the structure of air entrained concrete using a flatbed scanner", *Cement Concrete Res.*, **35**, 2041-2046.
Zhang, Z., Ansari, F. and Vitillo, N. (2005), "Automated determination of entrained air-void parameters in hardened concrete", *ACI Mater. J.*, **102**(1), 42-48.

CC